Interdisciplinary Neurosurgery: Advanced Techniques and Case Management 26 (2021) 101307

Contents lists available at ScienceDirect

Interdisciplinary Neurosurgery: Advanced Techniques and Case Management

journal homepage: www.elsevier.com/locate/inat

Tissue segmentation in histologic images of intracranial aneurysm wall

Annika Niemann *, Anitha Talagini, Pavan Kandapagari, Bernhard Preim, Sylvia Saalfeld

Department for Simulation and Graphics, Otto-von-Guericke University of Magdeburg, Magdeburg, Germany

ARTICLE INFO

Keywords:
Intracranial aneurysm
Histology
Segmentation

ABSTRACT

We qualitatively compare three image segmentation techniques (filter and threshold-based segmentation, texture-based clustering and deep learning) for histologic images of intracranial aneurysms. Due to remodeling of the vessel wall and aneurysm formation, the tissue is highly diverse. Only the deep learning segmentation provided semantic information about the segmented tissue. The other segmentation techniques were designed to segment areas of different textures and tissues, respectively. Therefore, in contrast to the deep learning approach, they did not require knowledge of all tissue types possible occurring in intracranial aneurysms. Rare tissue classes were missed by the deep learning segmentation, but the resolution of the deep learning segmentation was better than the ground truth segmentation. Overall, the deep learning segmentation of ten classes achieved a test accuracy of 60.68%.

1. Introduction

Intracranial aneurysms are pathological deformations of vessels in the brain, which can rupture with fatal consequences. Aneurysms are developed by remodelling of the vessel wall.

Tissue collected during surgery interventions can be used for histologic images of the intracranial aneurysm wall. These images provide useful insight into the structure and development of intracranial aneurysm walls on a cellular level. Understanding of the process in the aneurysm wall might be useful for further development of aneurysm treatment. For an analysis and further processing of the image, a segmentation of the histologic images is useful. The images are subdivided into different textures or tissue parts. Especially due to the large image size and many small details of histologic images manual segmentation are very time consuming. Therefore, computer supported segmentations are desired to analyse larger amounts of histologic images. In this work, three segmentation approaches are compared and their individual advantages and disadvantages are explored.

Histologic images are used in aneurysm research to understand the underlying processes of aneurysm development and rupture [1,2]. Based on findings in histologic images, it is assumed that high wall shear stress leads to proinflammatory signaling in endothelial cells. That recruits macrophages at the area of high wall shear stress. These macrophages secrete proteases that disrupt the internal elastic lamina and the collagen matrix. During aneurysm growth, the collagen type changes from predominant type IV,V,VI to predominant type I. Additionally, the orientation of the fibers changes [3]. Cebral et al. [4] found that wall degeneration and rupture were associated with increased inflammation in the aneurysm wall. A lack of intact endothelium and presence of organizing thrombus was also connected with inflammation. These analyses might be enhanced by automatic segmentation of intracranial aneurysm wall tissue. While not yet common in aneurysm research, segmentations for other tasks using histologic images exist. These will be discussed in the following.

Kather et al. [5] trained a classifier on images of eight tissue types found in human colorectal cancer. They calculated several features describing the texture in the images. The classification of the tissue types had an accuracy of 87.4%.

We segmented histologic images with three techniques: image classification based on filter and threshold operations, clustering based on texture features and deep learning.

2. Materials and methods

Three intracranial aneurysms were collected post mortem. The aneurysms were embedded in paraffin and sliced. The slices were stained with hematoxylin and eosin stain and digitalized with a Hamamatsu Nanozoomer (Hamamatsu Photonics, Hamamatsu, Japan). Overall, 177 histologic images were available. Next, 21 images were manually segmented into background and 9 different tissue classes. The classes are

* Corresponding author.
E-mail addresses: annika.niemann@ovgu.de (A. Niemann), anitha.talagini@st.ovgu.de (A. Talagini), pavan.kandapagari@ovgu.de (P. Kandapagari), bernhard.preim@ovgu.de (B. Preim), sylvia.saalfeld@ovgu.de (S. Saalfeld).

https://doi.org/10.1016/j.inat.2021.101307
Received 7 April 2021; Received in revised form 21 June 2021; Accepted 29 June 2021
Available online 11 July 2021

Table 1
Comparison of different segmentation approaches for histologic images.

Segmentation approach	Filter and threshold based	Texture analysis	Deep learning
focus	edges (e.g. nuclei outline) colour	textures/ patterns	user defined classes
speed	slow	very slow	fast
result influenced by	expected number of clusters minimum cluster size	selected features	training data no control over learned features
characteristics	robust against unseen tissue types/pathologies	robust against unseen tissue types/ pathologies	semantic information about tissue sections limited by available training data can only detect known tissue types
possible usage	guiding visual exploration distinguish nuclei rich and nuclei free areas	identify clusters	detect predefined tissue classes

inflammatory cells, myointimal hyperplasia, red thrombus, white thrombus, degenerated wall, decellularized organizing thrombus, organizing thrombus, mixed textures and intact wall. These were previous described by Niemann et al. [6].

2.1. Filter- and threshold-based segmentation

The first segmentation uses standard image processing algorithms. Two analyses of the images are performed: an edge-based analysis and an intensity-based analysis. The first step in the edge-based analysis is the enhancement of edges using the Prewitt filter. Using morphological operations, the edges are merged into larger areas. Most of the edges inside the aneurysm tissue occur due to the presence of nuclei. The described edge-based analysis detects nuclei-rich areas. The threshold-based analysis uses Otsu's method to segment the image with eight thresholds. The results of both analyses are combined, yielding an over-segmentation with many small areas. Areas are combined with their neighbouring small areas until either each segmented area is larger than a minimum size or until the number of different areas is below the maximum allowed number of areas. The parameters are not independent from each other and have to be adjusted according to the size and number of tissue changes visible in the image. Using a manual segmentation of the aneurysm's outer and inner contour, the background was set to zero.

2.2. Texture analysis and cluster

The second approach is an unsupervised machine learning approach: k-means clustering. For this purpose, the images are divided into overlapping 50 × 50 pixels large patches. For each patch, 249 features are calculated; i.e. 83 different features for the patch itself and its surrounding area, approximated twice as a 100 × 100 and a 150 × 150 pixels large patch. Two kinds of features were selected: features, which have been determined as useful for histologic image segmentation [5] and features based on the nuclei. For the nuclei detection and shape analysis, we used the approach by Glaßer et al. [7]. The optimal number of clusters was determined using the Calinski-Harabasz criterion. With k-means clustering, the images were divided into 37 clusters. After a visual inspection of the clustering result, several clusters were merged. One of the clusters detected by the algorithm contained all wall parts with no or few nuclei. This cluster was further divided using Otsu's method with two automatic thresholds. The result was smoothed with a median filter.

2.3. Deep learning approach

The images were too large to be used as a whole. Therefore, they were split up in 256 × 256 patches. Nine tissue classes and one background class were defined. From all patches, 7314 patches were selected. The patches were chosen to reduce the class imbalance; especially a large amount of patches solely consisting of background was removed. The data was split into 60:20:20 for training, test and validation. A neural net following the U-net design [8] with eighteen layers and using the Adam optimizer was trained to perform the segmentation. To account for the imbalanced classes, categorical cross-entropy was used. The net was trained for 50 epochs.

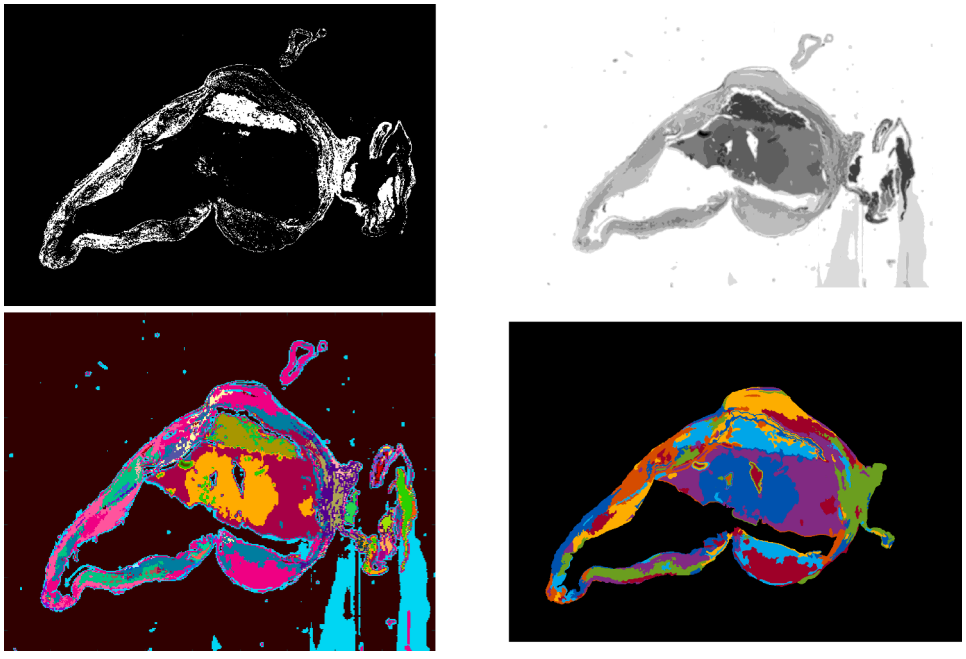

Fig. 1. Filter and threshold-based classification, after Prewitt Filter and morphological operations (top left), after threshold-based segmentation (top right), combination of both approaches (bottom left) and final classification (top right).

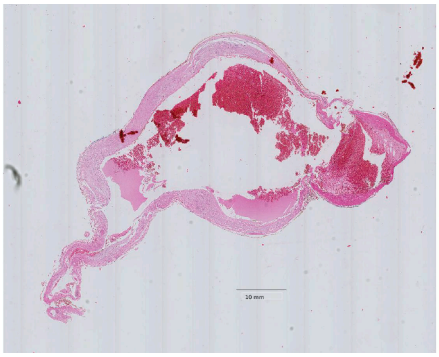

Fig. 2. Original image, 9402 × 7577 pixel, resolution of 0.92 µm per pixel.

Fig. 3. Result of image segmentation based on cluster.

3. Results

Each of the approaches has different characteristics as summarised in Table 1. The segmentation slightly differs between the approaches. The thrombus is segmented with all three approaches. Only the deep learning segmentation provides labels for the segmentation. In the other approaches labelling (for example of the segmented thrombus) has to be done manually. Deep learning is restricted to the classes presented in the training data while the other approaches can be used on data with different tissue classes or pathologies.

Fig. 1 shows the results of the segmentation of the image shown in Fig. 2 using the Prewitt filter, morphological operations and threshold-based segmentation.

An example for the result of the cluster algorithm is shown in Fig. 3. The grey values do not have a semantic meaning and are only used to illustrate the different segments. The cluster based segmentation often shows one cluster at the outline of the aneurysm wall.

The deep learning approach has an accuracy of 60.68%. Visual inspections of the images showed that the accuracy calculation has limited expressiveness in this case as the ground truth has mislabelled pixels. These occur because of small gaps in the tissue which are impractical to capture with manual segmentation but are detected by the deep learning segmentation. Examples of the predicted segments are shown in Fig. 4. The red thrombus and myointimal hyperplasia achieved the best results. Moderate results were achieved for white thrombus, intact wall and infiltrating blood. Rare classes like organizing thrombus (OT) and decellularized OT were not identified by the network. The decellularized OT was mostly segmented as white thrombus.

4. Discussion

Each algorithm has to be adjusted to the specific segmentation task.

The image processing required fine-tuning of the minimum object size in the classification and the expected number of objects in an image.

Clustering had problems with discriminating between tissue with no or few nuclei. As the results of clustering strongly depend on the selected features with other features this problem might be overcome.

The results of the deep learning segmentation heavily depends on the number of training data and the quality of the training data.

The visual inspection of the deep learning-based classification revealed that the net was able to learn a more detailed classification than the ground truth showed. This was especially visible for the background. Small gaps between the tissue were not segmented manually. Still, the deep learning classification was able to correctly identify these as background. Being superior to the ground truth has a negative impact on the accuracy. Manual segmentation with the same level of detail as provided by the deep learning net is too time-consuming and impractical. However, the segmentation yields clear borders between different tissue types. These are not able to reflect slow transitions between tissue classes.

The deep learning approach suffered from the limited number of training examples. The distribution of the classes was highly imbalanced, further complicating the problem. Intracranial aneurysm walls show a wide variation of tissues. The high number of classes is

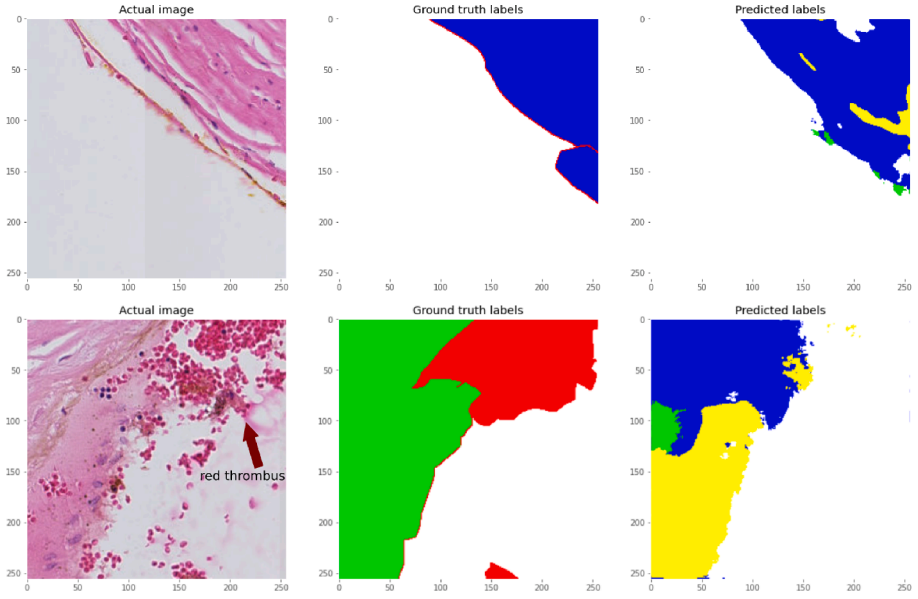

Fig. 4. Examples of deep learning segmentation; blue: myointimal hyperplasia, red: red thrombus, green: degenerated wall, blue: myoinitmal hyperplasia, yellow: white thrombus.

challenging for deep learning-based approaches.

For this application, working with patches is necessary due to the image resolution, but not optimal. Splitting the image into patches might be a disadvantage, as often only 1–2 classes are visible in a patch. Some information, e.g. the position in the image, is lost. As the different tissues are more likely to appear in certain places, like a plaque inside the vessel, the patch-based approach could omit relevant information.

The optimal choice for automatic segmentation depends on the specific task.

Supervised machine learning algorithms like the deep learning algorithm used here, are limited by the reliability of the ground truth they are trained with. Manually labelling the images is a time-consuming task. The manually generated ground truth and therefore the deep learning segmentation favours larger areas compared to the other algorithms.

The advantage of the image processing and the cluster algorithm is their flexibility. Especially in pathological structures like intracranial aneurysms, the tissue shows a high variation and differs from healthy tissue. The semantic deep learning segmentation restricts the possible findings of tissue classes and might not detect unusual variations that are lacking in the training data.

5. Conclusion

We compared three different segmentation methods. The deep learning segmentation can segment and label several classes. But it requires definition of suitable tissue classes and manual annotation of a large training datasets. While the deep learning segmentation is fast, the necessary preparation (data collection, annotation and training of the neural net) is very time-consuming. Texture-analysis and filter-and threshold-based segmentation do not require the definition of tissue classes and can segment new tissue types or pathologies.

CRediT authorship contribution statement

Annika Niemann: Conceptualization, Software, Visualization, Writing - original draft. **Anitha Talagini:** Software, Visualization. **Pavan Kandapagari:** Software, Visualization. **Bernhard Preim:** Supervision. **Sylvia Saalfeld:** Data curation, Resources, Supervision, Writing - review & editing.

Declaration of competing interest

The authors declare that they have no known competing financial interests or personal relationships that could have appeared to influence the work reported in this paper.

Acknowledgements

This work is partly funded by the German Research Foundation (SA 3461/2-1, BE 6230/2-1) and the Ministry of Economics, Science and Digitization of Saxony-Anhalt within the Forschungscampus STIMULATE (Grant No. I 117). We thank Thomas Hoffmann, Katja Jachau, Elisabeth Eppler and Martin Skalej for providing the patient data.

Compliance with ethical standards All procedures performed in studies involving human participants were in accordance with the ethical standards of the institutional and/or national research committee and with the 1964 Helsinki declaration and its later amendments or comparable ethical standards. For this type of study formal consent is not required.

References

[1] B.E. Grüter, S. Wanderer, F. Strange, G. Boillat, D. Täschler, J. Rey, D.M. Croci, D. Grandgirard, S.L. Leib, M. von Gunten, S.D. Santo, H.R. Widmer, L. Remonda, L. Andereggen, E. Nevzati, D. Coluccia, J. Fandino, S. Marbacher, Patterns of neointima formation after coil or stent treatment in a rat saccular sidewall aneurysm model, Stroke 52 (3) (2021) 1043–1052, https://doi.org/10.1161/STROKEAHA.120.032255.

[2] S. Marbacher, J. Marjamaa, K. Bradacova, M. von Gunten, P. Honkanen, U. Abo-Ramadan, J. Hernesniemi, M. Niemelä, J. Frösen, Loss of mural cells leads to wall degeneration, aneurysm growth, and eventual rupture in a rat aneurysm model, Stroke 45 (1) (2014) 248–254, https://doi.org/10.1161/STROKEAHA.113.002745.

[3] J. Frösen, J. Cebral, A. Robertson, T. Aoki, Flow-induced, inflammation-mediated arterial wall remodeling in the formation and progression of intracranial aneurysms, Neurosurg. Focus 47 (2019) 1–21, https://doi.org/10.3171/2019.5.FOCUS19234.

[4] J. Cebral, E. Netti, B. Chung, F. Mut, V. Sippola, B. Rezai Jahromi, R. Tulamo, J. Hernesniemi, M. Niemela, A. Robertson, J. Frosen, Flow conditions in the intracranial aneurysm lumen are associated with inflammation and degenerative changes of the aneurysm wall, Am. J. Neuroradiol. 38 (2016) 119–126, https://doi.org/10.3174/ajnr.A4951.

[5] J. Kather, C.-A. Weis, F. Bianconi, S. Melchers, L. Schad, T. Gaiser, A. Marx, F. Zöllner, Multi-class texture analysis in colorectal cancer histology, Sci. Rep. 6 (2016) 27988, https://doi.org/10.1038/srep27988.

[6] A. Niemann, S. Voß, R. Tulamo, S. Weigand, B. Preim, P. Berg, S. Saalfeld, Complex wall modeling for hemodynamic simulations of intracranial aneurysms based on histologic images, Int. J. Comput. Assist. Radiol. Surg. doi:10.1007/s11548-021-02334-z.

[7] S. Glaßer, T. Hoffmann, A. Boese, S. Voß, T. Kalinski, M. Skalej, B. Preim, Virtual inflation of the cerebral artery wall for the integrated exploration of oct and histology data, Comput. Graph. Forum 35 (2017) 57–68, https://doi.org/10.1111/cgf.12994.

[8] O. Ronneberger, P. Fischer, T. Brox, U-net: Convolutional networks for biomedical image segmentation, in: N. Navab, J. Hornegger, W.M. Wells, A.F. Frangi (Eds.), Medical Image Computing and Computer-Assisted Intervention – MICCAI 2015, Springer International Publishing, Cham, 2015, pp. 234–241.